Biomechanics and Modeling in Mechanobiology (2026) 25:2
https://doi.org/10.1007/s10237-025-02027-5

ORIGINAL PAPER

An in silico mechanoregulatory model of depth-dependent adaptations to mechanical loading in intact and damaged cartilage: a proof of concept study

Seyed Ali Elahi[1,2,3] · Rocio Castro-Viñuelas[1,2,4,6] · Petri Tanska[5] · Lauranne Maes[1,3] · Nele Famaey[1,3] · Rami K. Korhonen[5] · Ilse Jonkers[1,2,4,6]

Received: 5 June 2025 / Accepted: 19 October 2025

Abstract

Osteoarthritis induces profound structural degeneration of articular cartilage, with existing treatments remaining largely ineffective. This study pioneers a mechanoregulatory model utilizing histology-based finite element analysis to predict depth-dependent glycosaminoglycan (GAG) adaptations in both intact and damaged human cartilage under mechanical loading. Uniquely calibrated through rigorous one-week longitudinal in vitro experiments in intact cartilage, our model correctly predicts depth-dependent GAG content adaptation, also in damaged cartilage. Notably, the model reveals potential effects of fluid velocity and dissipated energy on an increase in GAG content, while highlighting the degenerative effects of maximum shear strain under physiological loading conditions. Interestingly, it replicates enhanced GAG production in damaged cartilage, consistent with our experimental observations. Beyond advancing the fundamental understanding of mechanical loading in cartilage homeostasis, this innovative model offers a robust platform for in silico trials, enabling the development of personalized rehabilitation protocols to optimize mechanical loading strategies for degenerative joint diseases. Our work represents a significant leap forward in leveraging computational tools to address the challenges of osteoarthritis treatment. All findings are based on human explants from one donor and should be interpreted as preliminary proof-of-concept.

Keywords Cartilage mechanobiology · Finite element modeling · Glycosaminoglycan (GAG) adaptation · Mechanoregulatory algorithm · Depth-dependent tissue response · In silico and in vitro integration

1 Introduction

Osteoarthritis (OA) is the leading cause of locomotor disability worldwide, affecting over 535 million people worldwide as of 2020 (Steinmetz et al. 2023). Characterized by debilitating joint pain and reduced mobility (Quicke et al. 2022), OA poses a significant public health challenge with profound socioeconomic implications. As the global population ages, the prevalence of OA is projected to surge, potentially resulting in an annual loss of 15 million Quality-Adjusted Life Years—comparable to the impacts of major diseases like cardiovascular conditions and cancer (Heinegård and Saxne 2011). This escalating burden underscores the urgent need for innovative therapeutic strategies, as developing effective curative or preventive treatments for OA remains a significant, unmet challenge (Glyn-Jones et al. 2015).

OA is a multifactorial joint disease involving alterations in articular cartilage, subchondral bone, and synovial

Seyed Ali Elahi and Rocio Castro-Viñuelas contributed equally to this work.

✉ Seyed Ali Elahi
seyedali.elahi@kuleuven.be

1 Institute for Physics-Based Modeling for In Silico Health, KU Leuven, Leuven, Belgium

2 Department of Movement Sciences, KU Leuven, Leuven, Belgium

3 Mechanical Engineering Department, KU Leuven, Leuven, Belgium

4 Department of Development and Regeneration, Skeletal Biology and Engineering Research Center, KU Leuven, Leuven, Belgium

5 Department of Technical Physics, University of Eastern Finland, Kuopio, Finland

6 Division of Rheumatology, University Hospitals Leuven, Leuven, Belgium

Published online: 12 December 2025

inflammation (Li et al. 2017). Cartilage degeneration, marked by the loss of its complex mechanobiological properties, is a hallmark of OA (Cucchiarini et al. 2016). Articular cartilage is essential for structural support, impact absorption, and smooth joint articulation (Ngwangwa 2024). Its extracellular matrix (ECM), a complex, solid-fluid composite synthesized by chondrocytes, is critical for cartilage's weight-bearing capacity and its mechanical integrity (Petitjean et al. 2023). The ECM comprises depth-dependent layers of proteoglycans (PGs) and collagen fibers, which interact to maintain cartilage functionality. Glycosaminoglycan (GAG) chains, covalently linked to PGs, are highly negatively charged and form a hydrated, gel-like structure that resists compression. The interaction between GAGs, collagen fibers, and the interstitial fluid contributes to the tissue's unique mechanical properties, enabling it to withstand loading during locomotion (Mohammadi et al. 2013) and maintain cartilage homeostasis.

Mechanical loading is fundamental to preserving the function and structure of the ECM. Physiological loading enhances cartilage integrity by promoting chondrocyte function through fluid flow-assisted nutrient delivery and energy dissipation, as evidenced by previous experimental studies (Mohammadi et al. 2013; Swartz and Fleury 2007; Abdel-Sayed et al. 2014; Nasrollahzadeh et al. 2019). The depth-dependent structure of the ECM modulates the mechanical environment around chondrocytes, maintaining their phenotype and supporting local ECM production across cartilage thickness (Murakami et al. 2007).

However, when cartilage undergoes structural degradation and damage, or is subjected to abnormal mechanical loading, localized strains and stresses disrupt the mechanical microenvironment around the chondrocytes. This disturbance triggers catabolic cellular processes and disorganizes the ECM, leading to mechanical failure of its components (Rahman et al. 2023). The resulting degenerative cascade involves collagen fibril degradation and fibrillation, PG depletion, and altered tissue hydration (Elahi et al. 2023). Increased fluid velocity further exacerbates ECM degeneration by causing the extrusion of small GAG fragments from the tissue (Mow et al. 2005; Sah et al. 1991), disrupting collagen fibril organization and accelerating matrix breakdown (Buckwalter 1992; Men et al. 2017; Saarakkala et al. 2010). Despite these insights, the precise role of local mechanical factors, such as tissue strain and fluid flow, in driving these changes in intact and damaged cartilage remains poorly understood.

Physics-based modeling techniques offer promising approaches to explore the complex interplay between mechanical loading and time- and depth-dependent changes in cartilage ECM constituents. Adaptive finite element (FE) models, in particular, enable us to connect macro-level cartilage loading to local tissue mechanics, including strains, stresses, and fluid dynamics. When combined with time-dependent adaptive algorithms, these models can already predict ECM degeneration based on constituent failure criteria (Orozco et al. 2018). In these models, tissue stresses or strains are compared to experimentally determined thresholds for ECM constituent failure, and the resulting changes in tissue structure, composition, and mechanical properties are predicted. Our recently developed Cartilage Adaptive REorientation Degeneration (CARED) model integrates key mechanisms of mechanics-driven degeneration, including collagen fibril reorientation, collagen loss, PG depletion, and changes in tissue hydration (Elahi et al. 2021a). By eliminating individual degenerative mechanisms, we simulated 'virtual knock-out' scenarios and identified the distinct contributions of various degenerative mechanisms to cartilage tissue failure (Elahi et al. 2023). Current models, however, predominantly focus on degenerative processes, neglecting the concurrent regenerative responses that occur under mechanical loading. The absence of regenerative mechanisms in existing models restricts their ability to fully capture the dynamic nature of cartilage adaptation and, in particular, their potential to predict the impact of altered mechanical loading on an increase in cartilage constituents.

In this study, we bridged this gap by establishing a model-based relationship between physiological mechanical loading and depth-dependent mechanobiological changes in intact human cartilage explants. We quantify the contributions of key mechanical factors—maximum shear strain, fluid velocity, and dissipated energy—to biological adaptations, particularly GAG content changes, observed in in vitro bioreactor experiments under mechanical loading. Leveraging our experimental data on loading-induced alterations in fibril orientation and GAG content, we developed a novel mechanoregulatory algorithm using histology-based FE analysis. This algorithm can predict degeneration and an increase in GAG content throughout the cartilage thickness. Following rigorous calibration and validation against longitudinal in vitro experiments, the model successfully captures the effects of tissue damage and compromised mechanical integrity in damaged cartilage on ECM adaptation.

Our mechanoregulatory model not only enhances the fundamental understanding of mechanical loading's role in cartilage homeostasis, but also serves as a robust platform for designing interventions that prevent structural cartilage degeneration and increase GAG content, paving the way for developing personalized rehabilitation protocols and mechanical loading strategies to optimize joint health.

2 Materials and methods

This study integrated advanced, histology-informed in silico modeling with dedicated in vitro longitudinal mechanical loading experiments to formulate a mechanoregulatory

algorithm describing depth-dependent cartilage adaptation under mechanical loads in human intact samples to then predict cartilage adaptations in damaged samples that were verified experimentally. Further methodological details are provided in the sections below.

2.1 Experimental study

Figure 1 provides an overview of the experimental study, which provided the experimental data informing the FE simulations.

2.1.1 Ethics statement

Informed consent and ethical approval of the University Hospitals Leuven Ethics Committee and Biobank Committee (Leuven, Belgium) (S56271) were obtained before performing this study.

2.1.2 Human articular cartilage harvesting and creation of defect

A total of 16 healthy human cartilage explants were harvested from the femoral head of an 80-year-old female donor with no history of OA, undergoing hip replacement surgery for osteoporotic or malignancy-associated fracture (Fig. 1A). All samples were harvested from the weight-bearing area of the femoral head. First, cartilage was dissected into fragments using a scalpel and then rinsed in phosphate-buffered saline (PBS) supplemented with 1% (vol/vol) antibiotic/antimycotic (Gibco). The cartilage fragments were cut with an 8 mm disposable biopsy punch (Robbins Instruments). In half

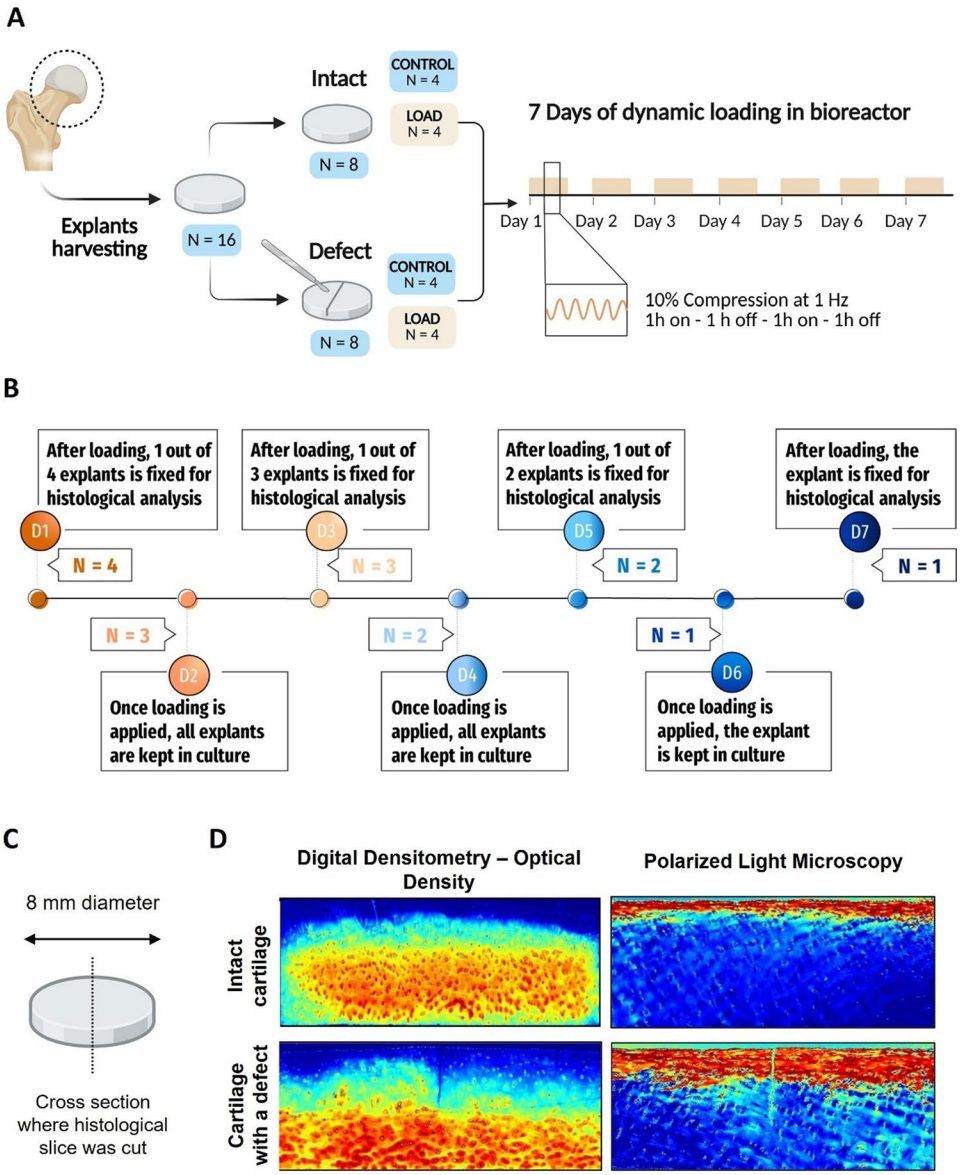

Fig. 1 Experimental workflow and example of raw digital densitometry (DD) and polarized light microscopy (PLM) results. **A** Schematic of the established workflow for applying long-term, ex vivo compressive loading to human articular cartilage explants both in the absence and in the presence of a defect. **B** Both intact and damaged cartilage explants were loaded for 7 days and fixed for quantitative histological measurements at days 1, 3, 5 and 7. **C** Illustration showing a cartilage explant and the location where histological sections were taken. **D** Digital densitometry and polarized light microscopy were used to quantify local GAG content and fibril orientation, respectively. ROI: region of interest, where the data are used for further analysis

of the explants, a cut (defect) through half of the depth of the sample was made with a scalpel and a metal ring to ensure a consistent defect depth across samples, while the remaining explants were left intact. All samples were cultured for 24 h in DMEM/F12 (Gibco), 10% fetal bovine serum (FBS, Gibco), 1% (vol/vol) antibiotic/antimycotic (Gibco), and 1% L-glutamine (Gibco) at 37 °C and 5% CO2 humidified atmosphere before starting the loading experiments.

2.1.3 Dynamic loading in bioreactor

In vitro mechanical stimulation was applied to articular cartilage explants in the ElectroForce® BioDynamic 5210 bioreactor (TA Instruments) with the accompanying WinTest® Software, inside an incubator at 37 °C and with 5% CO2, as previously described (Castro-Vinuelas et al. 2024). All elements of the loading chambers were gas sterilized before use. Cartilage explants were positioned in the loading chamber with the upper layer of the cartilage facing up while maintaining sterile conditions. The explant was secured between the two surfaces of the sample holder. Once closed, the loading chambers were filled with culture medium (DMEM/F12 + 10% FBS + 1% antibiotic/antimycotic + 1% L-glutamine) and placed in the bioreactor. The applied loading protocol consisted of 1 hour of 10% sinusoidal compressive strain (compression) at 1 Hz + 1 hour of free swelling + 1 hour of 10% compression at 1 Hz + 1 hour of free swelling. 10% compressive strain was defined based on the sample thickness (Fig. 1A) measured daily before the loading, using a Leica M50 Stereo Microscope equipped with a DFC425 C Digital Microscope Camera. The samples were gently stabilized from the sides to avoid compression of the tissue. No load was applied on the top or bottom surfaces. For each loaded explant, thickness was measured at three locations (central and two peripheral points), and the average was reported (Table 1). For each of the intact and damaged groups, half of the explants were maintained under free swelling conditions in an incubator at 37 °C and 5% CO2 as unloaded controls.

2.1.4 Quantitative measurements of GAG content and collagen fibril orientation

On day 1, day 3, day 5, and day 7, two loaded explants (one intact and one with a defect) and two unloaded controls (one intact and one with a defect) were harvested for quantitative histological measurements (Fig. 1B). Explants were rinsed with PBS and fixed with 4% formaldehyde in PBS for 24 h at 4 °C. Then, samples were decalcified in 0.5 M EDTA in PBS pH 7.5 for 5 days at 4 °C, changing the EDTA solution daily. On the 6th day, explants were washed in running tap water for 3 h and submerged in methanol for 24 h before paraffin embedding. Cartilage sections of 3 µm were harvested from the central cross section of explants (Fig. 1C) for staining, and 18 sections were prepared per sample.

GAG content and collagen fibril orientation were measured as described in a previous study (Fig. 1D) (Ebrahimi et al. 2022): Briefly, for measurements of GAG content by Digital Densitometry (DD), sections were dewaxed, rinsed in tap water, and stained with safranin-O for 5 min. After a 5 min wash under running tapwater, slides were air dried for 10 min, dehydrated with 4 washes in ethanol, and mounted on a microscope slide. Stained sections were then photographed using a standard light microscope (Nikon Microphot FXA, Nikon Co., Tokyo, Japan) with a pixel size of 3.09 × 3.09 µm. Imaging was performed with a CCD camera (Hamamatsu ORCA-ER, Hamamatsu Photonics, Hamamatsu, Japan) and a monochromator ($\lambda = 492 \pm 5$ nm), which was calibrated using neutral filters spanning a wide range of optical densities from 0 to 3.0.

For the evaluation of fibril orientation angle, unstained sections were imaged by a custom-designed Polarized Light Microscopy (PLM). The system consisted of a microscope body (Leitz Ortholux II POL light microscope, Leitz Wetzlar, Wetzlar, Germany), a light source with a monochromator ($\lambda = 630 \pm 30$ nm, Edmund Optics Inc., Barrington, NJ, USA), crossed polarizers (Techspec optics® XP42-200, Edmund Optics, Barrington, NJ, USA), and a monochrome camera (BFS-U3-88S6M-C FLIR Blackfly® S, FLIR

Table 1 Average thickness values for the 8 loaded cartilage samples measured before loading at each loading day

Sample		Thickness at day 1 (mm)	Thickness at day 2 (mm)	Thickness at day 3 (mm)	Thickness at day 4 (mm)	Thickness at day 5 (mm)	Thickness at day 6 (mm)	Thickness at day 7 (mm)
Load Intact	1	2.7	2.7	2.8	2.7	2.6	2.6	2.7
	2	3.3	3.1	3.2	3.3	3.1	Harvested	Harvested
	3	3.1	3.2	3.0	Harvested	Harvested	Harvested	Harvested
	4	1.9	Harvested	Harvested	Harvested	Harvested	Harvested	Harvested
Load Defect	1	2.4	2.2	2.3	2.5	2.5	2.4	2.3
	2	3.1	3.0	3.1	2.9	3.1	Harvested	Harvested
	3	2.1	2.1	2.1	Harvested	Harvested	Harvested	Harvested
	4	2.8	Harvested	Harvested	Harvested	Harvested	Harvested	Harvested

Systems Inc., Wilsonville, OR, USA, pixel size 3.5 µm × 3.5 µm) with a 2.5× magnification lens. The angle dependency of the observed light intensity induced by the collagen fibrils and the collagen network structure allows determining pixel-wise fibril angle and parallelism index (anisotropy) via Stokes parameters and Michelson's contrast method (Rieppo et al. 2008).

For each sample, we measured GAG content and fibril orientation data within a rectangular 2 mm wide region of interest (ROI) spanning throughout the tissue thickness (Fig. 1D): the ROI was positioned in the middle of the explant for the intact explants, and it was positioned symmetrically to the cut for the defect explants. Depth-wise profiles were then obtained by averaging over the 18 sections prepared for each sample in the ROI (Matlab R2022b, Mathworks Inc., MA, USA). To this end, the delimitation lines between the superficial, middle, and deep zones were determined using collagen fibril orientation maps from polarized light microscopy of intact day-1 samples, where orientation profiles reflect the original tissue state. Zones were defined as superficial (10% depth; fibrils predominantly parallel to the surface), middle (25% depth; random fibril orientation), and deep (65% depth; fibrils predominantly perpendicular to the surface). Using day-1 intact samples avoided confounding effects of defect creation, loading, or culture and ensured physiologically representative zone definitions. These thickness values were subsequently used to divide the sections into the three zones, allowing for the averaging of GAG content and fibril orientation within each zone in the ROI for further depth-wise analysis.

2.1.5 Statistical analysis

Data analysis and graphical presentation were performed with GraphPad Prism version 8. GAG content and fibril angle data averaged over depth were compared between conditions at each time point or cartilage layer by paired 2-tailed Student's test or Wilcoxon test in case of non-normal distribution. P values of pairwise comparisons are indicated in the graphs. Model assumptions were further checked by a Shapiro-Wilk test, QQ plots, and homoscedasticity plots. The homogeneity of variance was evaluated by standardized residuals versus fit plots. P values of less than 0.05 were considered significant. Statistical analyses were performed across histological sections ($n = 18$ per explant) within each group. As only one donor was included, results reflect within-sample variation and should be interpreted with caution regarding generalizability.

2.2 In silico modeling

Fig. 2 provides an overview of the development, calibration, and validation of the in silico modeling workflow.

2.2.1 Histology-based FE model definition

To assess the specific mechanical parameters that influence GAG content adaptations across the cartilage geometry, histology-based FE models were constructed for the eight loaded cartilage explants, consisting of four intact and four defect samples (Fig. 2A). The sample-specific models comprised cylindrical geometries with dimensions determined from measurements in the stereomicroscope. For modeling the defect samples, a surface cut of 20 µm width was created, comparable to the thickness of the scalpel used to create the surface cut on the defect explant, extending until half of the explant model thickness. The contact between the two adjacent surfaces of the cut was defined as surface-to-surface contact. Free fluid flow was allowed through the cut surfaces by assigning a zero-pore pressure boundary condition.

To model the mechanical behavior of articular cartilage, a 3D fibril-reinforced poroelastic (FRPE) material model was used (Elahi et al. 2021b). The histology-based FE models were implemented with sample-specific depth-dependent fibril orientation using data from PLM measurements (Fig. 2B). Depth-dependent fluid content, decreasing from the top surface to the bottom surface, was based on the literature (Elahi et al. 2021a), as we did not have the sample-specific data. The bottom surface of the explants was constrained against vertical translation, while both top and bottom surfaces were permitted to undergo radial expansion. A single cycle of sample-specific sinusoidal compressive deformation, in accordance with the applied deformation within the bioreactor, was applied to the top surface of the model (Fig. 2C). This loading was used as a representative of 1 day of the in vitro loading experiment. The fluid was allowed to flow through the side surface (pore pressure = 0).

The intact and defect samples were meshed using 24,962 and 27,756 linear pore pressure continuum elements (element type C3D8P), respectively (Abaqus/Standard software 2022 by Dassault Systèmes Simulia Corp, USA – Fig. 2A). A biased mesh seeding was employed to achieve finer element sizes near the open surfaces of the model, where fluid pressure and deformation gradients are larger. A mesh convergences analysis was conducted, using half, twice, and four times the selected number of elements. Simulations with higher mesh densities revealed no significant differences in deformation gradient, stress and fluid velocity distributions, indicative that the FE model outcomes (i.e., DE, MSS, and FV) used within the mechano-regulatory algorithm were not affected.

To identify sample-specific material properties – i.e., the constants of the FRPE material model (Elahi et al. 2021b) – an inverse parameter fitting approach was employed (Fig. 2D). The reaction force calculated at the bottom surface of the FE models was iteratively matched

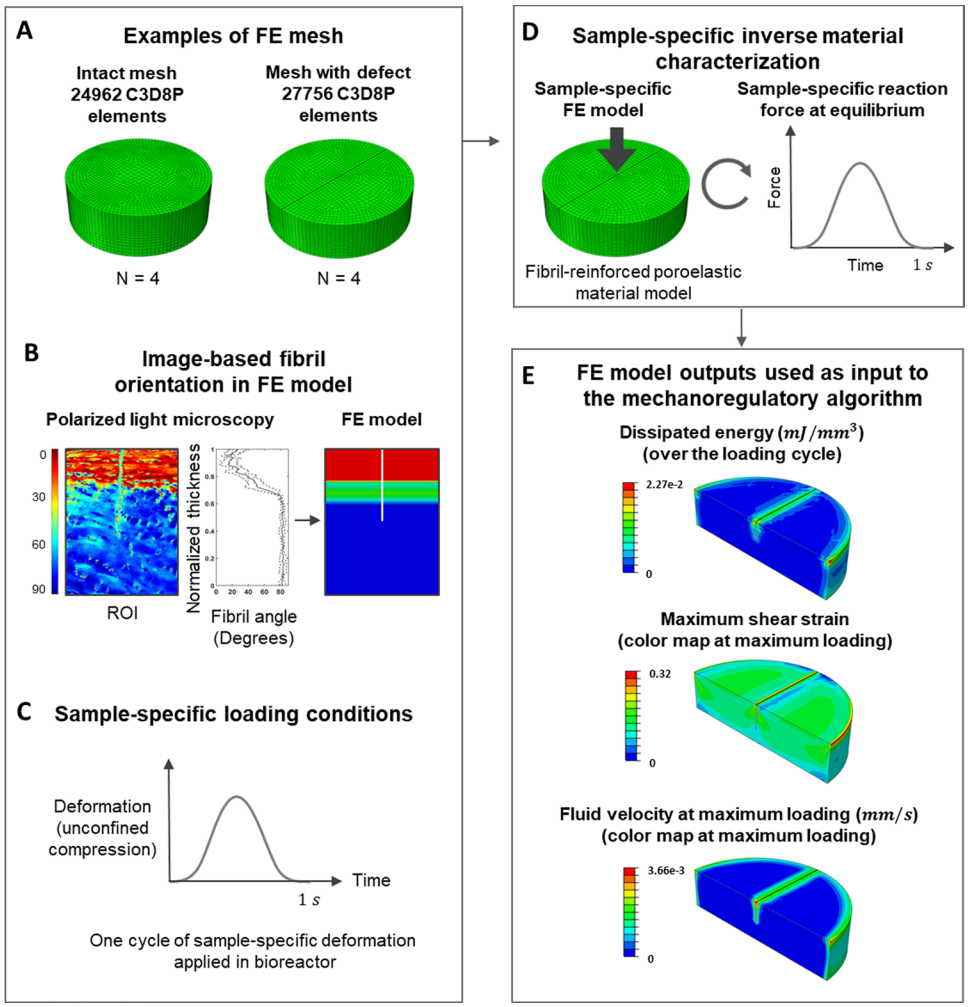

Fig. 2 Histology-based FE modeling workflow. **A** Examples of FE mesh, **B** sample-specific histology-based fibril orientation implemented in the FE model from the PLM measurements, **C** one cycle of sample-specific unconfined compression deformation applied to the explant, **D** Inverse material characterization to obtain the sample-specific material constants of FRPE material model and **E** examples of the three FE model outputs over the cartilage explants

to the measured reaction force of the corresponding cartilage sample within the bioreactor by altering the material constants. Unlike our earlier work (Elahi et al. 2021b), where stress-relaxation tests combined with optical tracking of lateral displacements were used to maximize parameter sensitivity, the present bioreactor setup did not allow optical measurements due to chamber humidity and design complexity. Therefore, material parameters were identified by fitting the model-predicted reaction force to the experimentally measured force after the samples reached equilibrium during the second loading step. This corresponds to the equilibrium response of the explant under cyclic loading and is analogous to the "steady-cycle" state used in Elahi et al. (2021b). Therefore, the fitted FRPE parameters correspond to the equilibrium mechanical state of each explant, and a single representative loading cycle adequately describes the steady-cycle mechanics used by the mechanoregulatory algorithm. To this end, the "lsqnonlin" optimization function (Matlab software R2022b by Mathworks Inc., MA, USA) was used.

2.2.2 FE model output processing

Three mechanical parameters, as outputs of FE models, namely the dissipated energy (DE), maximum shear strain (MSS) and fluid velocity (FV), were evaluated across the explants' geometry (Fig. 2E). Both the MSS and FV were recorded at each integration point and time increment throughout the loading cycle, with specific information about the calculation method for MSS available in (Elahi et al. 2021a). The DE per unit volume was calculated over the loading cycle by summing the absolute areas of hysteresis loops obtained for the components of stress versus deformation gradient in each integration point. The three parameters were averaged over the cartilage thickness within the specific sample region (ROI as shown in Fig. 1D).

A non-localization theory as described in Elahi et al. (2021a); Párraga Quiroga et al. (2017) was used to avoid localization of FE model outputs. The non-localized FE model output at each intended integration point (ip) of the FE model was obtained as follows:

$$\mathrm{FEout}_{\mathrm{nl,ip}} = \frac{\sum_{\mathrm{intp}=1}^{nip} \omega_{\mathrm{ip,\,intp}}(\mathrm{FEout}_{\mathrm{intp}})}{\sum_{\mathrm{intp}=1}^{n\mathrm{ip}} \omega_{\mathrm{ip,\,intp}}} \quad (1)$$

where $\mathrm{FEout}_{\mathrm{nl,ip}}$ is the non-localized FE model output that can be $\mathrm{DE}_{\mathrm{nl,ip}}$, $\mathrm{MSS}_{\mathrm{nl,ip}}$ or $\mathrm{FV}_{\mathrm{nl,ip}}$ and int$p$ and $n$ip are the index and the total number of integration points in the FE model. $\omega_{\mathrm{ip,\,intp}}$ is the Gauss weighting function at the intended integration point (ip) with respect to other integration points (intp) and was obtained as follows:

$$\omega_{\mathrm{ip,intp}} = \frac{1}{(2\pi)^{3/2} l^3} \exp\left[-\frac{\sqrt{\left(x_{\mathrm{intp}} - x_{\mathrm{ip}}\right)^2 + \left(y_{\mathrm{intp}} - y_{\mathrm{ip}}\right)^2 + \left(z_{\mathrm{intp}} - z_{\mathrm{ip}}\right)^2}}{2l^2}\right] \quad (2)$$

where x_j, y_j, and z_j are the coordinates of intended and other integration points and l is the characteristic length, which is a property related to the scale of the microstructure. This parameter was selected to be equal to the superficial layer thickness (Párraga Quiroga et al. 2017).

The time average of $\mathrm{MSS}_{\mathrm{nl,ip}}$ and $\mathrm{FV}_{\mathrm{nl,ip}}$ in the load-unload cycle were calculated as follows:

$$\mathrm{FEout}_{\mathrm{nl,ip,cycle}} = \frac{\sum_{t=1}^{\mathrm{ToT}} \mathrm{FEout}_{\mathrm{nl,ip},t}\mathrm{INC}_t}{T_{\mathrm{cycle}}} \quad (3)$$

where $\mathrm{FEout}_{\mathrm{nl,ip,cycle}}$ can be $\mathrm{MSS}_{\mathrm{nl,ip,cycle}}$ or $\mathrm{FV}_{\mathrm{nl,ip,cycle}}$. T_{cycle} is the total time of the loading cycle. TOT and INC_t are the total number of time points (t) during each loading step and the duration of each time increment in the FE model. $\mathrm{FEout}_{\mathrm{nl,ip},t}$ is the FE model output in each time increment of the FE model, which can be $\mathrm{MSS}_{\mathrm{nl,ip},t}$ or $\mathrm{FV}_{\mathrm{nl,ip},t}$.

2.2.3 Mechano-regulatory algorithm formulation

To ensure comparability with the histological measurements, the depth-dependent, non-localized FE model outputs were obtained and averaged over the same ROI as defined for the histological sections (refer to Fig. 1D). Drawing inspiration from a mechano-adaptive model proposed for tendon tissue (Notermans et al. 2021), the resulting averaged parameters were employed to establish three normalized factors (as provided in Eqs. (4) to (6) and visualized in Fig. 3), indicative of their positive or negative effects on the GAG content.

As suggested in the literature (Abdel-Sayed et al. 2014; Nasrollahzadeh et al. 2019; Moghadam et al. 2015), dissipated energy was assumed to stimulate GAG production. Therefore, its positive effect was simulated as:

$$\mathrm{NF}_{\mathrm{DE}} = \begin{cases} \frac{1}{1+e^{-\alpha\left[\left(\mathrm{DE}_{nl,\mathrm{ip}}/\mathrm{TP}_{\mathrm{DE}}\right)\beta - C_1\right]}} & \text{if } \mathrm{DE}_{nl,\mathrm{ip}} \le \mathrm{TP}_{\mathrm{DE}} \\ \frac{1}{1+e^{-\alpha\left[\left(2-\mathrm{DE}_{nl,\mathrm{ip}}/\mathrm{TP}_{\mathrm{DE}}\right)\beta - C_1\right]}} & \text{if } \mathrm{DE}_{nl,\mathrm{ip}} > \mathrm{TP}_{\mathrm{DE}} \end{cases} \quad (4)$$

where $\alpha = 75$, $\beta = 0.15$, $C_1 = 0.07$ are shape parameters (Notermans et al. 2021) and $\mathrm{TP}_{\mathrm{DE}} = 3.96\left(\mu\mathrm{J/mm}^3\right)$ is a transition point at which the dissipated energy stimulates the maximum GAG production. This value was determined by averaging the dissipated energy over one loading cycle during the equilibrium state of intact cartilage explants on the initial day of loading within the bioreactor – the condition

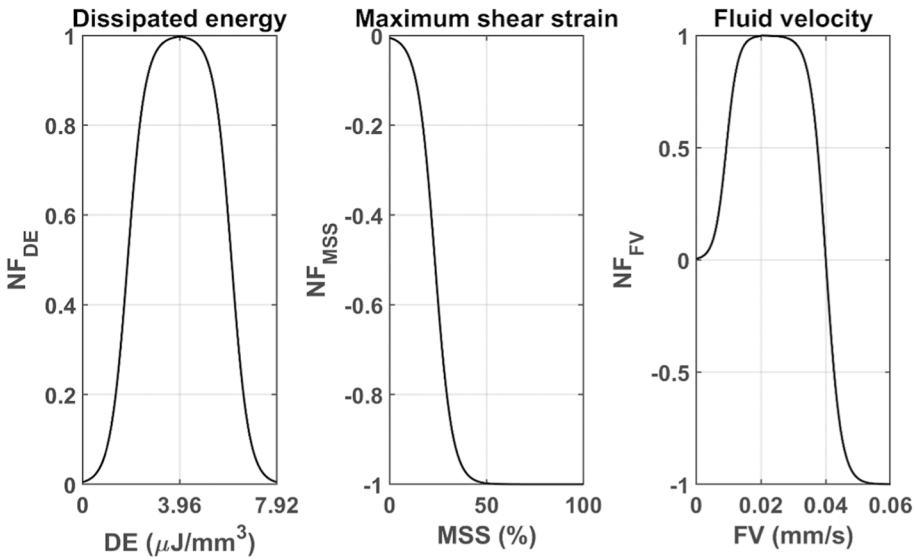

Fig. 3 Normalized effects of FE model outputs on the change in GAG content demonstrated by normalized factors. The curves were obtained using Eqs. (4) to (6). Positive and negative values demonstrate GAG production and degeneration effects, respectively

that is most representative the mechanical behavior of native healthy cartilage.

According to the literature (Orozco et al. 2018; Elahi et al. 2021a; Eskelinen et al. 2019), maximum shear strain is associated with PG depletion and loss of GAG chains. Therefore, we defined its negative effect on GAG content as:

$$\mathrm{NF_{MSS}} = \frac{-1}{1 + \mathrm{e}^{-\alpha\left[\left(\mathrm{MSS}_{nl,\mathrm{ip,cycle}}/\mathrm{TP_{MSS}}\right)\beta - C_1\right]}} \tag{5}$$

where $\mathrm{TP_{MSS}} = 0.5$ represents the point at which MSS reaches its most significant negative impact (maximum degeneration) on GAG content, a value obtained from a preceding study (Orozco et al. 2018).

Fluid flow within the cartilage tissue has been reported to either positively or negatively affect GAG content: a moderate fluid flow (moderate FV) can facilitate nutrient and growth factors delivery while imposing a moderate hydrostatic fluid pressure is believed to enhance chondrocyte GAG production (Swartz and Fleury 2007). Conversely, excessive fluid velocity was reported to have a negative impact on cartilage homeostasis and elicit the extrusion of small GAG protein fragments (Orozco et al. 2018). We defined the combined impact of FV on GAG content as follows:

$$\mathrm{NF_{FV}} = \begin{cases} \dfrac{1}{1+\mathrm{e}^{-\alpha\left[\left(\mathrm{FV}_{nl,\mathrm{ip,cycle}}/\mathrm{TP_{FV}}\right)\beta - C_1\right]}} & \text{if } \mathrm{FV}_{nl,\mathrm{ip,cycle}} \le \mathrm{TP_{FV}} \\ \dfrac{2}{1+\mathrm{e}^{-\alpha\left[\left(2-\mathrm{FV}_{nl,\mathrm{ip,cycle}}/\mathrm{TP_{FV}}\right)\beta - C_1\right]}} - 1 & \text{if } \mathrm{FV}_{nl,\mathrm{ip,cycle}} > \mathrm{TP_{FV}} \end{cases} \tag{6}$$

where $\mathrm{TP_{FV}} = 0.02(\mathrm{mm/s})$ represents the transition point at which FV has its maximum positive effect on GAG production and assumed as half of the degradation threshold ($\mathrm{FV} = 0.04(\mathrm{mm/s})$) proposed in an earlier study (Orozco et al. 2018).

To evaluate the significance of each FE output on the change in overall GAG content due to the mechanical loading, the normalized factors were multiplied by weighting factors and change factors were obtained as:

$$\mathrm{CF}_i = k_i NF_i \tag{7}$$

where k_i represents the weighting factors of the FE model outputs (i.e., k_{DE}, k_{MSS} and k_{FV}). To reflect the experimentally observed depth-dependent changes in GAG content, the change factors were summed and multiplied to a depth-dependent rate of GAG change and the total change factor was obtained as:

$$\mathrm{CF_{total}}_j = \left(\sum \mathrm{CF}_i\right) \times \mathrm{GAG_{depth}}_j \tag{8}$$

where $\mathrm{GAG_{depth}}_j$ represents the depth-dependent rate of change in GAG content where j can be the superficial, middle or deep layer (i.e., $\mathrm{GAG_{depth_{sup}}}$, $\mathrm{GAG_{depth_{mid}}}$ and $\mathrm{GAG_{depth_{deep}}}$).

Finally, the depth-dependent GAG content in each day of loading was predicted as:

$$\mathrm{GAG}_{jd} = \mathrm{GAG}_{j(d-2)} + \mathrm{CF_{total}}_{jd} \cdot \Delta\mathrm{GAG}_{j(d-2)} + \Delta\mathrm{GAG_{Bd}} \tag{9}$$

where d represents the day of loading in the bioreactor (days 1, 3, 5 and 7) and $\Delta\mathrm{GAG_{Bd}}$ is the basal change in the GAG content. Given that the present mechano-regulatory model primarily aims to replicate the GAG content variations driven by mechanical parameters, $\Delta\mathrm{GAG_{Bd}}$ encompasses the free swelling effect on GAG content within the explants. This parameter was derived by calculating the difference between the depth-dependent GAG contents of the control samples across two consecutive DD measurement days. The GAG content at day zero ($\mathrm{GAG_0}$), before the first loading, was considered as the measured GAG content using DD in the control sample at day 1.

2.2.4 Calibration, validation and sensitivity analysis of mechano-regulatory algorithm

To calibrate the mechano-regulatory algorithm, the six unknown parameters within Eqs. (7) and (8) – namelyk_{DE}, k_{MSS}, k_{FV}, $\mathrm{GAG_{depth_{sup}}}$, $\mathrm{GAG_{depth_{mid}}}$, and $\mathrm{GAG_{depth_{deep}}}$– were identified by fitting these parameters to optimally match the GAG content predictions from the mechano-regulatory algorithm to the experimental DD measurement results of the intact explants. To this end, the obtained outputs from the histology-based FE models of intact explants ($\mathrm{DE_{nl,ip}}$, $\mathrm{MSS_{nl,ip,cycle}}$, and $\mathrm{FV_{nl,ip,cycle}}$) were fed into the mechano-regulatory algorithm, initially employing an estimated set of the six parameters. To account for the variability in the explants at each loading day and estimate the loading effect on the changes in GAG content, both the experimental and the predicted GAG content by the model in the loaded samples were first normalized to the GAG content of the corresponding control sample and the normalized values were compared. Through an iterative process using the "lsqnonlin" optimization function in Matlab (Mathworks), the above-mentioned six parameters were optimized to fit the normalized GAG contents obtained from the algorithm to the corresponding experimental values.

To validate the mechano-regulatory algorithm, the identified parameters were applied in conjunction with histology-based FE models of the defect explants to predict GAG content in the loaded defect samples across the loading days. The predicted change in GAG results (based on Eq. (9)) in case of an impaired mechanical environment was then compared to the corresponding DD measurements.

Finally, the calibrated and validated mechano-regulatory algorithm enabled a parameter sensitivity analysis to explore the impact of each FE model output on mechanics-driven changes in GAG content – *i.e.,* CF_i values in Eq. (7). This entailed a comparison of average CF_i values over the cartilage thickness as well as their average across the superficial, middle and deep zones on the loading days, enabling the comparison of the significance of each FE output on the change in overall GAG content due to the mechanical loading.

3 Results

3.1 Loading-induced fibril reorientation in intact and damaged cartilage to inform the histology-based FE model development

A representative image obtained by PLM together with the measured fibril orientation over tissue depth in the ROI is shown in Fig. 4A. In the absence of mechanical stimulation, the presence of a defect resulted in decreased alignment of collagen fibrils with the cartilage surface (Fig. 4B), with this effect being significant in middle and deep layers at days 1, superficial and middle layers at day 3, all layers at day 5, and only deep layer at day 7 (Fig. 4C).

Mechanical loading induced collagen fibrils to align with the cartilage surface (as reflected by the decreased fibril angle) in intact samples, with this effect being significant at days 1 and 5 (Fig. 4B). Depth-dependent analysis shows this effect in all layers up to day 5 (except for the superficial layer on day 3 – Fig. 4C). However, disruption of the surface integrity due to a defect impaired the fibril reorientation upon loading as no significant changes in fibril angle were observed, on average, in the cartilage explants with a defect. As a result, fibrils were less aligned with the surface in the explants with a defect than intact explants, although not significantly on average (Fig. 4B). This suggests that loading in the presence of a defect could lead to disorganization of the collagen network, which may reduce tissue strength.

The obtained sample-specific depth-dependent fibril orientation before loading was used to inform the histology-based FE models of intact and defect explants (Fig. 2B).

3.2 Loading-induced changes in GAG content of intact and damaged cartilage to calibrate and validate the mechanoregulatory model

A representative image of the depth-dependent quantitative histology together with the measured GAG content over tissue depth in the ROI is shown in Fig. 5A.

In the absence of mechanical stimulation, the average GAG content over the ROI (Fig. 5B) decreased over time in both intact explants and explants with a defect. Interestingly, the presence of a defect in control explants significantly decreased the GAG content compared to the intact explants on day 1, day 3, and day 5. Depth-dependent analysis revealed that GAG content in control explants (Fig. 5C) increased with cartilage depth, further validating our measurements according to the literature (Saadat et al. 2006; Seitz et al. 2022).

Upon mechanical stimulation of intact explants, GAG content increased at all time points and was significantly higher than in control explants after 7 days of loading and throughout the tissue depth. Surprisingly, mechanical stimulation also increased the GAG content in the samples with a defect, reaching similar levels as intact cartilage explants. However, the presence of a defect in unloaded samples resulted in lower GAG content compared to unloaded intact explants in all cartilage layers during the first 5 days.

The measured GAG content in intact samples was used to calibrate the mechanoregulatory model parameters, and the measured GAG content in defect samples was used to validate the model predictions.

3.3 Calibration of mechanoregulatory algorithm using the experimental results of intact samples

The calibrated model effectively accounts for depth- and time-dependent changes in GAG content over 7 days of mechanical loading in the intact samples (see Fig. 6A). Specifically, the model exhibits a robust fit with root mean square error (RMSE) of 15.49% for the average GAG content throughout the cartilage thickness (see Fig. 6B). Table 2 shows the values of the identified weighting factors during the calibration process. Notably, the depth-dependent rate of GAG change (GAG_{depth_j}) increases from the deep to the superficial zone. More precisely, the rate of GAG change in the superficial zone is approximately twice that in the deep zone, indicating a pronounced depth-dependent variation in GAG turnover within the cartilage tissue. This suggests that mechanically induced changes in GAG content are more prominent in the superficial layer and gradually decrease with cartilage depth.

The parameters within the calibrated mechanoregulatory model enable us to decipher the distinct contributions of individual mechanical triggers to changes in GAG content. In Fig. 6C, we delineate the individual contribution of each FE model output to the depth-dependent GAG content changes over time, based on their corresponding change factors (i.e. CF_{DE}, CF_{MSS} and CF_{FV} that are functions of DE, MSS and FV defined in Eq. (7)). The mechanoregulatory model inherently defines DE as a positive, MSS as a negative, and *FV* as a bidirectional contributor to GAG adaptation. The novel outcome of our analysis

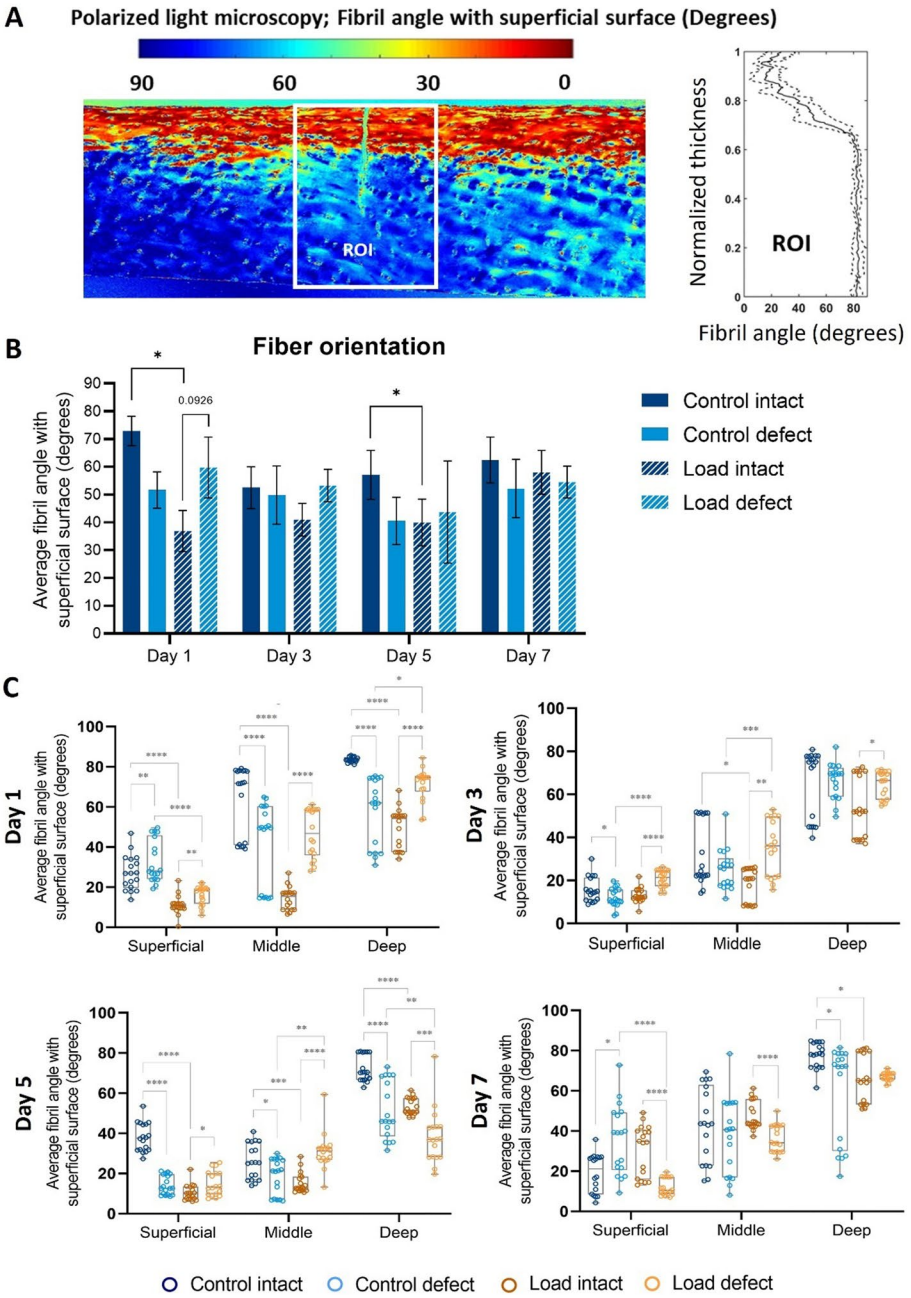

Fig. 4 Mechanical loading-induced fibril reorientation: **A** Representative image of polarized light microscopy analysis of a cartilage section with a defect and the selected region of interest (ROI). **B** Bar graph showing the average fibril angle with the superficial layer in intact cartilage sections and sections with a defect, both in the presence and absence of mechanical stimulation during 7 days of culture ($n = 18$ sections per sample). **C** Depth-dependent quantification of fibril reorientation in intact cartilage sections and sections with a defect, both in the presence and absence of mechanical stimulation during 7 days of culture ($n = 18$ sections per sample). $P < 0.05$ (*), $P < 0.01$ (**), $P < 0.001$ (***), $P < 0.0001$ (****)

lies in the relative magnitudes of these contributions: FV emerged as the dominant factor driving GAG changes across depths and time points, while DE had only a limited effect, and MSS played a comparatively minor role.

The results reveal that fluid velocity exerts a significant positive influence on GAG production, maintaining a consistent effect across various depths and time points, while dissipated energy exhibits a limited positive effect on GAG production. In contrast, the maximum shear strain negatively affects GAG content.

3.4 Validation of mechanoregulatory algorithm using the experimental results of defect samples

To validate the in silico model predictions, the mechanoregulatory algorithm was used to predict the depth-dependent changes in GAG content over time in defect samples – presenting an altered mechanical environment due to the surface cut. For this purpose, the weighting factors and depth-dependent rates of GAG change, calibrated for the intact

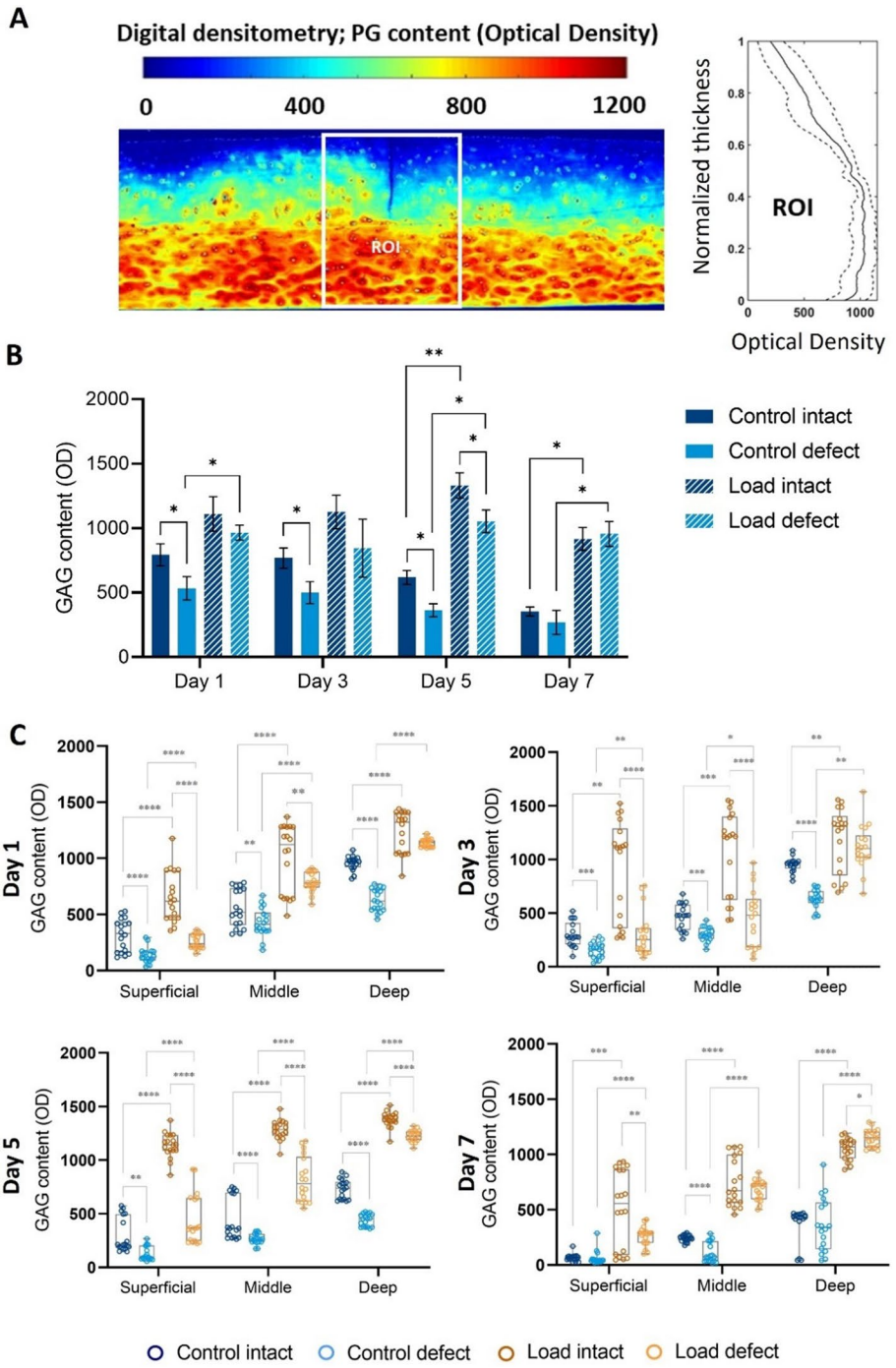

Fig. 5 Mechanical loading–induced changes in GAG content: **A** Representative image of digital densitometry analysis of a cartilage section with a defect and the selected region of interest (ROI). **B** Bar graph of GAG quantification in intact cartilage sections and sections with a defect, both in the presence and absence of mechanical stimulation during 7 days of culture ($n = 18$ sections per sample). **C** Depth-dependent quantification of GAG content in intact cartilage sections and sections with a defect, both in the presence and absence of mechanical stimulation during 7 days of culture ($n = 18$ sections per sample). $P < 0.05$ (*), $P < 0.01$ (**), $P < 0.001$ (***), $P < 0.0001$ (****)

explants (Table 2), were used together with the FE models' outputs (DE, MSS and FV) of the defect samples. The normalized depth-dependent experimental and model-predicted GAG content at different days of loading are compared in Fig. 7A. The RMSE of 13.50% for the average of the predicted GAG content over cartilage thickness (Fig. 7B). This is in the same range as RMSE after parameter calibration in the intact samples (15.49% in Fig. 6B). This result shows that the in silico model, even when calibrated with the data from the intact samples, can predict the mechanics-driven changes induced by a compromised mechanical environment in the defect samples.

To assess whether the compromised mechanical environment in the defect samples affected the contribution of the different FE model outputs to the observed changes in GAG content, we compared the values of their corresponding dept and time-dependent change factors (i.e., CF_{DE}, CF_{MSS} and CF_{FV} that are functions of DE, MSS and FV defined with

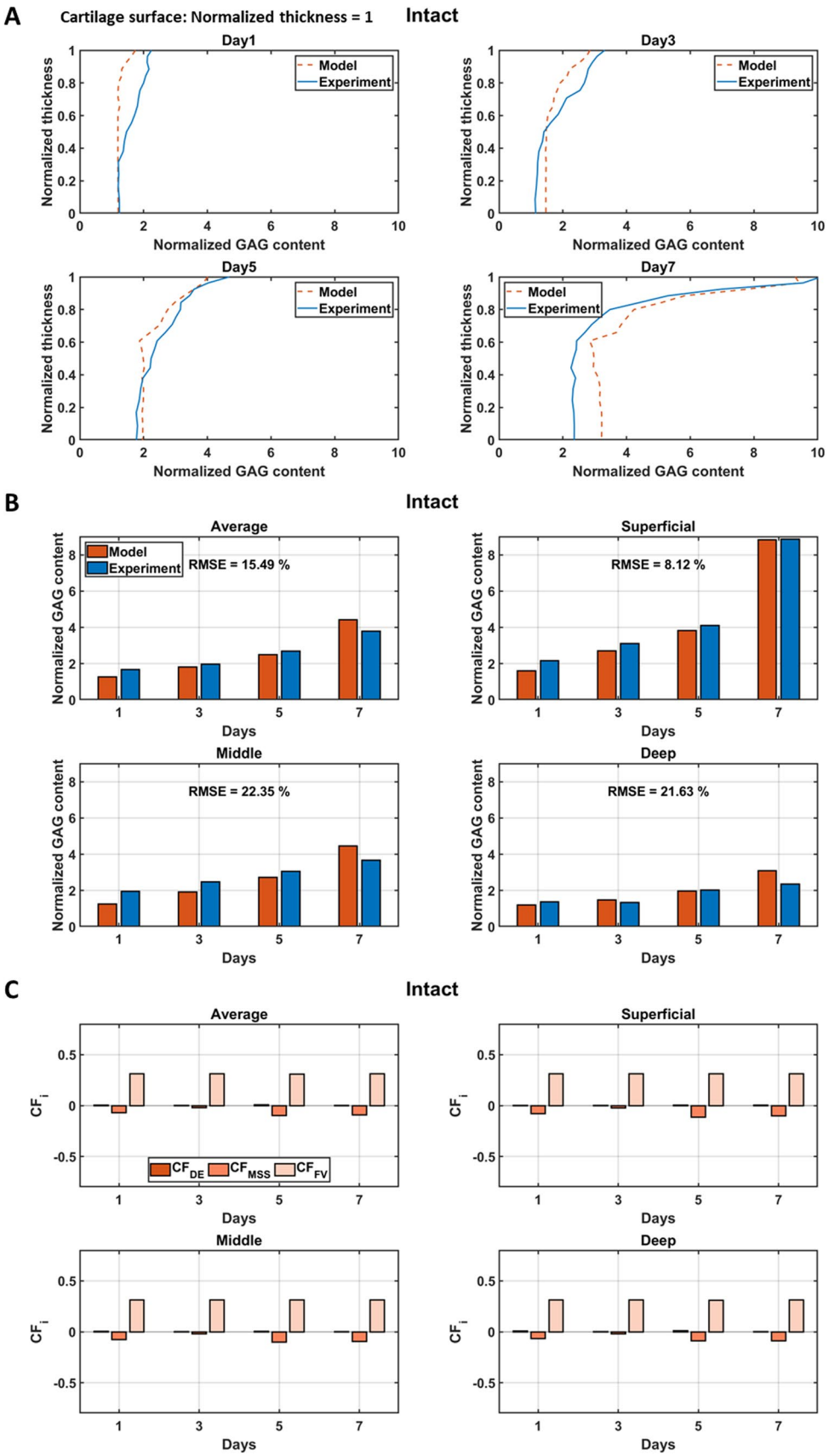

Fig. 6 In silico model, calibrated with intact explants, shows the contribution of mechanical micro-environment to the changes in GAG content changes. **A** The graph shows the optimal fit of the predicted depth-dependent normalized GAG content by the in silico model over several test days compared to the experimental observations (DD measurements). **B** A comparison between the mean value of the predicted normalized GAG content and the corresponding experimental values is shown. This comparison is made over the total cartilage thickness (average) and within the superficial, middle, and deep layers over the course of the test days. The quality of the fit is indicated by the RMSE values. **C** Contribution of the three mechanical parameters to the change in GAG content as reflected in the change factors

Table 2 Calibrated weighting factors and depth-dependent rates of GAG change in the in silico model

Parameter	Identified value following calibration using intact explant DD data
k_{DE}	0.63
k_{MSS}	2.83
k_{FV}	90.48
$GAG_{depth_{sup}}$	1.97
$GAG_{depth_{mid}}$	1.38
$GAG_{depth_{deep}}$	0.98

These parameters were adjusted to obtain the optimal fit between model predicted and experimental GAG content in intact samples – see Eqs. (7) and (8)

Eq. (7)) over the measurement days and cartilage thickness (Fig. 7C). The results show that, in contrast to the intact samples, DE had a significant positive effect on the defect samples in both the superficial and middle zones, with an increasing contribution in the superficial zone over the measurement days. However, the effect was minimal in the deep zone. On the other hand, MSS had a negative effect, with its significance decreasing from the superficial to the deep zone but an increasing contribution in the superficial zone over the measurement days. FV showed a significant positive effect over the entire cartilage depth, but in contrast to DE and MSS, its effect decreased in the superficial zone over the measurement days.

4 Discussion

Mechanical factors are vital for maintaining articular cartilage's structural integrity and functionality. However, excessive loading or abnormal joint mechanics can accelerate cartilage degradation, precipitating the onset and progression of OA (Bader and Salter 2011). Understanding which mechanical factors contribute to the degeneration and production of cartilage constituents in health and disease is crucial for designing personalized rehabilitation strategies to prevent or mitigate OA. By defining ranges of mechanical stimuli that promote GAG increase while avoiding excessive strain, the model offers a potential framework for defining loading-tailored rehabilitation. Such insights could help clinicians design exercise regimes optimized for individual cartilage conditions.

We achieved a significant advancement by developing an innovative in silico model that leverages a novel mechanoregulatory algorithm integrated within a histology-based FE modeling framework. This sophisticated modeling approach enabled us to identify and quantify the critical roles of maximum shear strain (MSS), fluid velocity (FV), and dissipated energy (DE) as pivotal mechanical parameters influencing depth-dependent ECM adaptation in both intact and damaged human cartilage explants. The added value of our modeling lies in its ability to simultaneously predict biological responses enhancing or degenerating cartilage constituents, a feature that is largely absent in existing models, which typically focus on degeneration alone. To this end, longitudinal in vitro experiments on intact human cartilage explants, and for the first time, on damaged cartilage explants, were conducted using our bioreactor setup to calibrate and validate the developed mechanoregulatory algorithm, respectively.

To maintain strict data–model consistency, this study used experimentally measured fibril orientation as input to the FE models, as fibril orientation has a major influence on predicted mechanical responses. We focused model calibration and validation on GAG adaptations, since measurable changes occur within the short timeframe of the experiments, whereas collagen turnover is extremely slow and no changes were expected during one week of culture (Elahi et al. 2021a). Nevertheless, the framework is modular and could be extended to include collagen adaptations in future studies with longer experimental durations and suitable validation data.

Our earlier modeling framework (Elahi et al. 2021a) relied on strict mechanical thresholds (e.g., a maximum shear strain limit) driving cartilage degradation. In contrast, the present approach extends the previous work to better align with observed mechano-adaptations by introducing three modifications to the mechano-regulatory formulation. First, rather than enforcing abrupt thresholds, the current framework applies gradual mechanoregulatory rules that allow for more continuous and therefore adaptations in GAG content. Second, in addition to maximum shear strain, we incorporated dissipated energy and fluid velocity as drivers of both GAG depletion and production, enabling the model to capture productive as well as degenerative responses. Finally, we introduced the ΔGAGBd parameter to represent baseline, steady-state changes in GAG content observed in our free-swelling controls that are not accounted for by mechanical stimuli. This formulation ensures that mechanical contributions are interpreted relative to intrinsic biochemical adaptations occurring during steady state that cannot be captured by loading-induced adaptations.

Calibrated using the intact explants' data, the model successfully predicted the overall experimentally observed increase in GAG production within defect explants subjected to mechanical loading (Figs. 6B and 7B).

Indeed, our experimental results emphasized the necessity of mechanical stimulation to maintain homeostatic GAG levels, not only in intact cartilage but also in cartilage with a defect. Our combined approach, blending in vitro experiments with in silico modeling, revealed that physiological

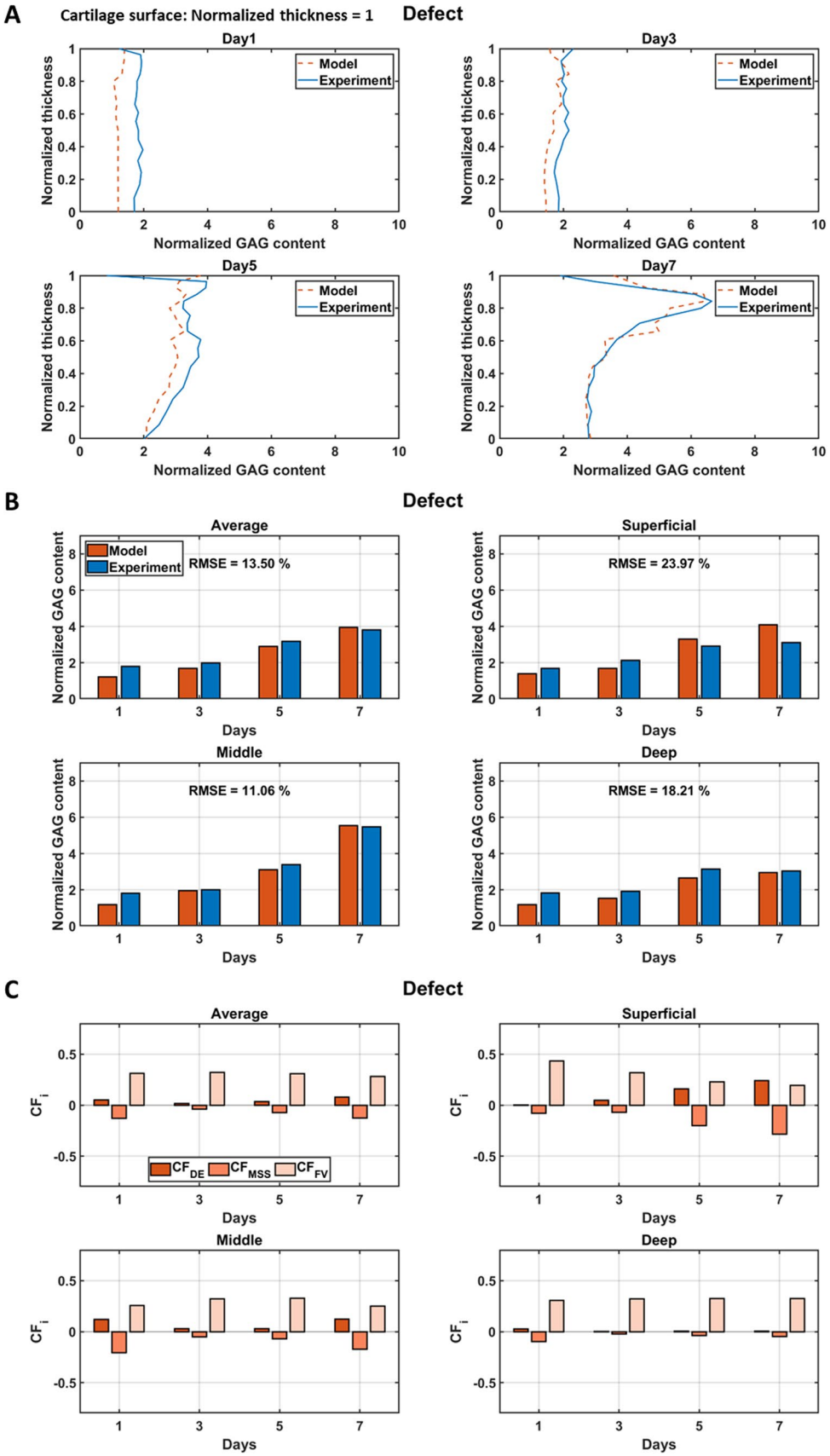

Fig. 7 In silico model, validated against explants with defect, can explain and predict depth-dependent changes in GAG content upon loading. **A** The graph shows the predicted depth-dependent normalized GAG content by the in silico model over several test days compared to experimental observations obtained through DD measurements. **B** A comparison is shown between the mean values of the predicted normalized GAG content and the corresponding experimental values. This comparison is made over the total cartilage thickness (average) and within the superficial, middle, and deep layers over the course of testing days. The RMSEs of the in silico model predictions are shown. **C** Contribution of the three mechanical parameters to the change in GAG content reflected in the change factors

cyclic loading optimally increases dissipated energy and fluid velocity, fostering proteoglycan synthesis.

In addition, the model demonstrated the ability to predict the depth-dependent adaptation in GAG content of defect cartilage explants following mechanical loading. The depth-dependent rates of GAG change were identified by incorporating sample-specific, experimentally measured depth-dependent fibril orientation into the finite element models (Table 2). The model parameters emphasized the more significant role of mechanics in driving changes in GAG content in the superficial zone compared to the middle and deep zones. Furthermore, the model showcased its predictive capacity by accurately mirroring the experimentally observed temporal variations in GAG content resulting from the mechanical loading of explants with a defect across the cartilage thickness. More specifically, the model can mimic the experimental observation that mechanical stimulation positively influenced GAG content even in the presence of a half-depth cartilage defect, with a more pronounced increase compared to intact cartilage.

The presence of a defect led to distinct GAG content alterations, with less pronounced increases in the superficial layer and more pronounced increases in the middle layer compared to intact explants (solid lines in Fig. 8) indicative of a shift in the mechanical environment favorable for GAG production in the middle layer. Remarkably, the in silico model accurately predicted these variations (dashed lines in Fig. 8), showcasing its ability to gage distinct mechanical conditions between intact and defect explants underlying the observed distinct GAG production in the different zones.

It is important to note that the sign of the mechanoregulatory contributions (positive for DE, negative for MSS, and bidirectional for FV) is inherent to the design of the model. The main findings of this study therefore concern the relative weights of these contributions, which were not predetermined but emerged from the calibration and validation against experimental data. These relative weights provide new insights into the predominant mechanical factors driving depth-dependent GAG adaptations, which is challenging to assess through experimental procedures alone. The analyses revealed that FV consistently emerged as the predominant contributor to changes in GAG content induced by physiological loading, promoting GAG production across all layers of intact explants and in the deep layer of defect explants (Figs. 6C and 7C). Depth-dependent differences were also evident: in defect explants, DE made a stronger relative contribution in the superficial layer (days 5 and 7), while MSS contributed more prominently to degeneration in the superficial (days 5 and 7) and middle layers (days 1 and 7). These differences can be explained by elevated shear strains around the defect, which not only increased the relative weight of MSS but also increased DE's contribution to GAG production.

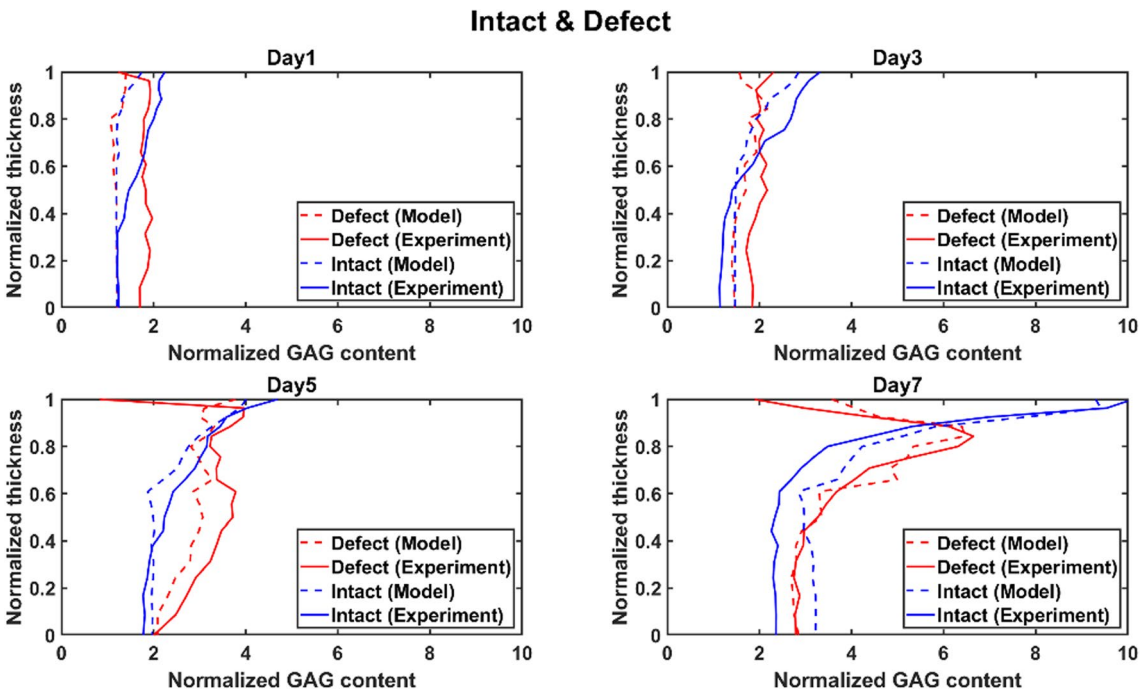

Fig. 8 In silico model can predict the temporal variations in depth-dependent GAG content resulting from the mechanical loading and defect. The graph shows the in silico model's predicted depth-dependent normalized GAG content over multiple testing days compared to experimental observations obtained through DD measurements for intact and defect explants

To evaluate the precision of predictions, a meticulous examination of the calibration process was conducted, assessing fitting quality, prediction errors, and potential discrepancies. The algorithm exhibited exceptional fit in the superficial layer, gradually diminishing with increasing cartilage depth. Although taking into account the sample-specific depth-dependent fibril orientation in the FE models, the predictions demonstrated varying precision across different depths, highlighting the importance of addressing sample-specific depth-dependent fluid content in future work.

To increase the clinical transferability, future research should focus on incorporating cutting-edge experiments using non-destructive imaging techniques and integrating biochemical-driven in silico models to enhance the non-destructiveness and comprehensiveness of our mechanoregulatory model. Advanced imaging modalities such as synchrotron-based imaging (Inamdar et al. 2017, 2021) promise to refine the model, allowing for more accurate parameter calibration. These techniques can offer valuable insights into cartilage microstructure strain and 3D composition under mechanical loading. MRI-based methods (Lee et al. 2023; Linka et al. 2021; Zevenbergen et al. 2018) on the other hand, allow for longitudinal tracking of changes in cartilage properties within a single sample due to their non-destructive nature. The current limitation of the model in considering the impact of biochemical factors observed in OA joints needs to be acknowledged, suggesting integration with existing in silico models focusing on biochemical and inflammatory aspects (Rahman et al. 2023; Eskelinen et al. 2020; Kosonen et al. 2023) to evolve to a comprehensive mechano-biochemical model.

Given our focus on developing the FE-based mechanoregulatory algorithm and its calibration and validation, along with the constraints of accessing non-OA human cartilage samples and conducting time-intensive and expensive longitudinal mechanical loading experiments, we used cartilage samples from a single donor. Therefore, for robust and conclusive extrapolation of the experimental findings, future studies should consider increasing the sample size. This approach would enable incorporating probabilistic modeling approaches to address input parameter variability, hence leveraging probabilistic instead of deterministic model outcomes. Furthermore, as validation was performed on explants from a single, aged donor, caution is warranted in extrapolating results. Age-related differences in matrix structure, cellular mechanosensitivity, and adaptations may affect the donor's specific adaptation patterns. Therefore, population-wide validation should be addressed in future work, testing multiple donors and disease stages. To maintain strict data–model consistency, this study used the measured collagen orientation as input to the sample-specific FE models and limited the model calibration and validation to GAG adaptations. Extension of the framework to collagen adaptation is feasible and represents an important direction for future work.

Although we made efforts to harvest samples from anatomically similar regions to minimize variability, the high number of explants required to test all experimental conditions posed logistical constraints. As a result, in this cross-sectional design, the precise anatomical location of each individual sample could not be fully accounted for. Importantly, the individual finite element simulations were informed by sample-specific parameters obtained from measured forces in the bioreactor and fibril orientation from microscopy. This approach helps account for potential between-sample variability in the mechano-regulatory adaptation formulation.

Ultimately, the in silico mechanoregulatory model holds significant potential to impact in vitro and in vivo experiments, unraveling the intricate interactions between mechanical loading and biological changes. In the context of tissue engineering, the model can optimize interventions by identifying the role of individual mechanical parameters in ECM adaptations under mechanical loading. This not only enhances therapy effectiveness, but also contributes to reducing reliance on animal experiments, addressing ethical concerns associated with them. Additionally, the model offers opportunities to optimize in vitro mechanobiological experiments, aiding in designing new OA rehabilitation approaches. This aligns with recent endeavors to advance in silico trials, which aim at simulating clinical conditions, predicting treatment outcomes, and thereby facilitating more informed and efficient clinical trials. As such, this work underscores the future potential of the model in understanding clinical conditions, predicting outcomes and advancing personalized rehabilitation and medicine approaches.

Acknowledgements We are grateful to the UZ Leuven nursing staff for their efforts to provide cartilage samples for this work and to Lies Storms for her help with cartilage sample preparation for histology.

Author contributions Conceptualization: SAE, RCV, IJ Methodology: SAE, RCV, PT, LM Investigation: SAE, RCV Visualization: SAE, RCV Supervision: NF, RK, IJ Writing—original draft: SAE, RCV Writing—review and editing: SAE, RCV, PT, LM, NF, RK, IJ.

Funding This work was supported by the Marie Skłodowska-Curie Individual Fellowship for CREATION project: MSCA-IF-2019-893771 (SAE), Flanders Research Foundation (FWO-Vlaanderen) junior postdoctoral fellowship 12Y7422N (RCV), KU Leuven Happy Joints project C14/18/077 (IJ, NF), FWO-Vlaanderen Happy Joints project G045320N (IJ) and FWO-Vlaanderen EOS excellence program Joint-Against OA G0F8218N (IJ).

Data Availability The raw data supporting the conclusions of this article will be made available by the authors upon request.

Declarations

Conflict of interest The authors declare no competing interests.

References

Abdel-Sayed P, Darwiche SE, Kettenberger U, Pioletti DP (2014) The role of energy dissipation of polymeric scaffolds in the mechano-biological modulation of chondrogenic expression. Biomaterials 35:1890–1897

Bader DL, Salter DM, Chowdhury TT (2011) Biomechanical influence of cartilage homeostasis in health and disease. Arthritis 2011:979032

Buckwalter JA (1992) Mechanical injuries of articular cartilage. Iowa Orthop J 12:50–57

Castro-Viñuelas R, Viudes-Sarrion N, Rojo-Garcia AV, Monteagudo S, Lories RJ, Jonkers I (2024) Mechanical loading rescues mechanoresponsiveness in a human osteoarthritis explant model despite Wnt activation. Osteoarthr Cartil

Conaghan PG, Corp N, Peat G (2022) Osteoarthritis year in review 2021: epidemiology & therapy. Osteoarthritis Cartilage 30:196–206

Cucchiarini M, De Girolamo L, Filardo G, Oliveira JM, Orth P, Pape D, Reboul P (2016) Basic science of osteoarthritis. J Exp Orthop 3:1–8

Ebrahimi M, Turkiewicz A, Finnilä MA, Saarakkala S, Englund M, Korhonen RK, Tanska P (2022) Associations of human femoral condyle cartilage structure and composition with viscoelastic and constituent-specific material properties at different stages of osteoarthritis. J Biomech 145:111390

Elahi SA, Tanska P, Korhonen RK, Lories R, Famaey N, Jonkers I (2021a) An in silico framework of cartilage degeneration that integrates fibril reorientation and degradation along with altered hydration and fixed charge density loss. Front Bioeng Biotechnol 9:529

Elahi SA, Tanska P, Mukherjee S, Korhonen RK, Geris L, Jonkers I, Famaey N (2021b) Guide to mechanical characterization of articular cartilage and hydrogel constructs based on a systematic in silico parameter sensitivity analysis. J Mech Behav Biomed Mater 124:104795

Elahi SA, Castro-Viñuelas R, Tanska P, Korhonen RK, Lories R, Famaey N, Jonkers I (2023) Contribution of collagen degradation and proteoglycan depletion to cartilage degeneration in primary and secondary osteoarthritis: an in silico study. Osteoarthr Cartil 31:741–752

Eskelinen AS, Mononen ME, Venäläinen MS, Korhonen RK, Tanska P (2019) Maximum shear strain-based algorithm can predict proteoglycan loss in damaged articular cartilage. Biomech Model Mechanobiol 18:753–778

Eskelinen AS, Tanska P, Florea C, Orozco GA, Julkunen P, Grodzinsky AJ, Korhonen RK (2020) Mechanobiological model for simulation of injured cartilage degradation via pro-inflammatory cytokines and mechanical stimulus. PLoS Comput Biol 16:e1007998

Glyn-Jones S, Palmer AJ, Agricola R, Price AJ, Vincent TL, Weinans H, Carr AJ (2015) Osteoarthritis. Lancet 386:376–387

Heinegård D, Saxne T (2011) The role of the cartilage matrix in osteoarthritis. Nat Rev Rheumatol 7(50–56):198

Inamdar SR, Knight DP, Terrill NJ, Karunaratne A, Cacho-Nerin F, Knight MM, Gupta HS (2017) The secret life of collagen: temporal changes in nanoscale fibrillar pre-strain and molecular organization during physiological loading of cartilage. ACS Nano 11:9728–9737

Inamdar SR, Prévost S, Terrill NJ, Knight MM, Gupta HS (2021) Reversible changes in the 3D collagen fibril architecture during cyclic loading of healthy and degraded cartilage. Acta Biomater 136:314–326

Kosonen JP, Eskelinen AS, Orozco GA, Nieminen P, Anderson DD, Grodzinsky AJ, Korhonen RK, Tanska P (2023) Injury-related cell death and proteoglycan loss in articular cartilage: numerical model combining necrosis, reactive oxygen species, and inflammatory cytokines. PLoS Comput Biol 19:e1010337

Lee W, Miller EY, Zhu H, Luetkemeyer CM, Schneider SE, Neu CP (2023) High frame rate deformation analysis of knee cartilage by spiral dual MRI and relaxation mapping. Magn Reson Med 89:694–709

Li MH, Xiao R, Li JB, Zhu Q (2017) Regenerative approaches for cartilage repair in the treatment of osteoarthritis. Osteoarthr Cartil 25:1577–1587

Linka K, Thüring J, Rieppo L, Aydin RC, Cyron CJ, Kuhl C, Merhof D, Truhn D, Nebelung S (2021) Machine learning-augmented and microspectroscopy-informed multiparametric MRI for the non-invasive prediction of articular cartilage composition. Osteoarthr Cartil 29:592–602

Men YT, Li XM, Chen L, Fu H (2017) Experimental study on the mechanical properties of porcine cartilage with microdefect under rolling load. J Healthc Eng 2017:2306160

Moghadam MN, Pioletti DP (2015) Improving hydrogels′ toughness by increasing the dissipative properties of their network. J Mech Behav Biomed Mater 41:161–167

Mohammadi H, Mequanint K, Herzog W (2013) Computational aspects in mechanical modeling of the articular cartilage tissue. Proc Inst Mech Eng H 227:402–420

Mow VC, Gu WY, Chen FH (2005) Structure and function of articular cartilage and meniscus. In: Mow VC, Huiskes R (eds) Basic orthopaedic biomechanics and mechano-biology, 3rd edn. LWW, Philadelphia, pp 181–258

Murakami T, Sakai N, Sawae Y, Okamoto M, Ishikawa I, Hosoda N, Suzuki E (2007) Depth-dependent compressive behaviors of articular cartilage and chondrocytes. In: Wada H (ed) Biomechanics at micro-and nanoscale levels, vol 4. World Scientific, pp 1–20

Nasrollahzadeh N, Karami P, Pioletti DP (2019) Control of dissipation sources: a central aspect for enhancing the mechanical and mechanobiological performances of hydrogels. ACS Appl Mater Interfaces 11:39662–39671

Ngwangwa H (2024) Cartilage and knee joint biomechanics. In: Nochehdehi AR, Thomas S, Nemavhola F, Maria HJ (eds) Cartilage tissue and knee joint biomechanics. Academic Press, Cambridge, pp 423–442

Notermans T, Tanska P, Korhonen RK, Khayyeri H, Isaksson H (2021) A numerical framework for mechano-regulated tendon healing - simulation of early regeneration of the Achilles tendon. PLoS Comput Biol 17:e1008636. https://doi.org/10.1371/journal.pcbi.1008636

Orozco GA, Tanska P, Florea C, Grodzinsky AJ, Korhonen RK (2018) A novel mechanobiological model can predict how physiologically relevant dynamic loading causes proteoglycan loss in mechanically injured articular cartilage. Sci Rep 8:15542

Párraga Quiroga JM, Wilson W, Ito K, Van Donkelaar CC (2017) The effect of loading rate on the development of early damage in articular cartilage. Biomech Model Mechanobiol 16:263–273

Petitjean N, Canadas P, Royer P, Noël D, Le Floc'h S (2023) Cartilage biomechanics: from the basic facts to the challenges of tissue engineering. J Biomed Mater Res A. https://doi.org/10.1002/jbm.a.37478

Rahman MM, Watton PN, Neu CP, Pierce DM (2023) A chemo-mechano-biological modeling framework for cartilage evolving in health, disease, injury, and treatment. Comput Methods Programs Biomed 231:107419

Rieppo J, Hallikainen J, Jurvelin JS, Kiviranta I, Helminen HJ, Hyttinen MM (2008) Practical considerations in the use of polarized light microscopy in the analysis of the collagen network in articular cartilage. Microsc Res Techniq 71:279–287

Saadat E, Lan H, Majumdar S, Rempel DM, King KB (2006) Long-term cyclical in vivo loading increases cartilage proteoglycan content in a spatially specific manner: an infrared microspectroscopic imaging and polarized light microscopy study. Arthritis Res Ther 8:R147

Saarakkala S, Julkunen P, Kiviranta P, Makitalo J, Jurvelin JS, Korhonen RK (2010) Depth-wise progression of osteoarthritis in human articular cartilage: investigation of composition, structure and biomechanics. Osteoarthr Cartil 18:73–81

Sah RL, Doong JY, Grodzinsky AJ, Plaas AH, Sandy JD (1991) Effects of compression on the loss of newly synthesized proteoglycans and proteins from cartilage explants. Arch Biochem Biophys 286:20–29

Seitz AM, Warnecke D, Dürselen L (2022) Cartilage biomechanics. In: Innocenti B, Galbusera F (eds) Human orthopaedic biomechanics. Academic Press, Cambridge, pp 147–168

Steinmetz JD, Culbreth GT, Haile LM, Rafferty Q, Lo J, Fukutaki KG, Cruz JA, Smith AE, Vollset SE, Brooks PM, Cross M (2023) Global, regional, and national burden of osteoarthritis, 1990–2020 and projections to 2050: a systematic analysis for the Global Burden of Disease Study 2021. Lancet Rheumatol 5:e508–e522

Swartz MA, Fleury ME (2007) Interstitial flow and its effects in soft tissues. Annu Rev Biomed Eng 9:229–256

Zevenbergen L, Gsell W, Chan DD, Vander Sloten J, Himmelreich U, Neu CP, Jonkers I (2018) Functional assessment of strains around a full-thickness and critical sized articular cartilage defect under compressive loading using MRI. Osteoarthr Cartil 26:1710–1721